applied sciences

MDPI

Article

An Experimental Comparative Study of Flat and Extended-Surface PCM Containers for Passive Cooling of Photovoltaic Panels

Turki Almudhhi * and Mahmoud Badawy Elsheniti

Mechanical Engineering Department, College of Engineering, King Saud University, Riyadh 11451, Saudi Arabia; mbadawy.c@ksu.edu.sa

* Correspondence: talmudhhi@ksu.edu.sa

Abstract

In this study, an experimental investigation was conducted to evaluate the thermal and electrical behavior of three photovoltaic panel configurations under controlled indoor solar irradiation of 600, 800, and 1000 W/m^2, considering both natural and forced convection to the surrounding air. The tested configurations included an uncooled reference panel (PV-1), a PCM-cooled panel incorporating a flat rear container (PV-2), and a proposed PCM-cooled panel equipped with an extended-surface rear container (PV-3). A PCM characterized by a phase change temperature range of 41–48 °C was employed. The results showed that the extended-surface PCM configuration associated with PV-3 provides a more effective passive cooling solution compared to the flat container design. Under natural convection, this thermal advantage of PV-3 became more pronounced, with a maximum temperature reduction of 15 °C at 1000 W/m^2 after 170 min of operation, compared to PV-2. Consequently, PV-3 achieved the highest electrical performance, delivering peak efficiency enhancements of 12.05% and 7.38% relative to PV-1 and PV-2, respectively, and average efficiency gains of 7.06% and 5.35% over the entire test period. Under forced convection, however, performance differences among the configurations were minimal because forced convection dominated the heat removal process, reducing the influence of the PCM.

Keywords: photovoltaic cooling; phase change material; indoor solar simulation; passive cooling; extended surfaces; natural and forced convection

1. Introduction

Photovoltaic (PV) systems have attracted considerable attention as a clean and sustainable energy source. Over the past two decades, PV systems have experienced remarkable growth, emerging as an essential part of the world's clean energy sector. However, their performance is strongly influenced by operating temperature. An increase in PV cell temperature leads to two major consequences: a reduction in electrical efficiency and the induction of thermal stress, which accelerates material degradation and shortens system lifespan [1,2]. According to projections by the Intergovernmental Panel on Climate Change, the global mean surface temperature may rise by up to 4 °C during the 21st century. Even modest temperature increases can significantly impact PV performance. For instance, a uniform temperature rise of 2 °C results in an estimated annual energy yield reduction of 0.74%, while a 5 °C increase leads to a decline of approximately 1.85% under Portuguese climatic conditions. These effects are expected to be more pronounced in hot regions, where elevated ambient temperatures further intensify thermal stress on PV modules [3].

Check for updates

Academic Editor: Maria Vicidomini

Received: 2 June 2026
Revised: 24 June 2026
Accepted: 25 June 2026
Published: 29 June 2026

Copyright: © 2026 by the authors. Licensee MDPI, Basel, Switzerland. This article is an open access article distributed under the terms and conditions of the Creative Commons Attribution (CC BY) license.

In extreme climates such as Riyadh, Saudi Arabia, the impact of temperature is even more evident. It has been reported that implementing cooling techniques can enhance PV power output by approximately 2–3.24% for every 1 °C reduction in panel temperature under severe summer conditions [4].

To address these challenges, various thermal management strategies have been investigated, including active and passive cooling techniques [5,6]. Among these, phase change materials (PCMs) have emerged as a promising passive solution for regulating PV panel temperature. PCMs absorb excess heat during phase transition without requiring additional energy input, making them an energy-efficient cooling approach. The effectiveness of a PCM largely depends on its melting temperature range, which must be carefully selected to match local climatic conditions and maximize annual system performance [7].

Despite their advantages, PCMs typically exhibit low thermal conductivity, which limits heat dissipation to the surroundings, particularly when thicker PCM layers are used [8]. It was found that after the melting process was completed, the hybrid PV-PCM module exhibited a PV panel temperature that was 3 °C higher than that of the reference module without cooling [9]. To overcome this limitation, researchers have explored various enhancements, including the incorporation of nanoparticles and hybrid cooling configurations, optimizing the configurations of the PCM enclosures [10].

Several experimental studies have demonstrated the potential of PCM-based cooling systems. Elsheniti et al. evaluated photovoltaic PCM (PV-PCM), photovoltaic thermal PCM (PVT-PCM), and low-concentration PVT-PCM systems in Riyadh under ambient temperatures ranging from 27 to 35 °C. They employed RT-42 as the PCM, with a melting range of 41–48 °C, suitable for local climatic conditions [11]. They reported that the PV-PCM configuration provided only marginal improvement in electrical efficiency, increasing from 13.56% to 13.64%, primarily due to insufficient natural cooling during the afternoon. In contrast, the PVT-PCM system required additional energy input to operate the cooling fluid pump. Liu et al. conducted indoor experiments using PCM nano-emulsions with phase transition temperatures of 29 °C and 38 °C as coolants in a photovoltaic thermal (PVT) module, operating under irradiance levels between 744 and 1134 W/m^2 [12]. They suggested that operating PCM nano-emulsions at lower flow rates is preferable, as it minimizes the required pumping power. However, they also observed that the overall electrical efficiency of the PVT system remained lower than that of a standalone PV panel.

Further improvements have been achieved through nanoparticle-enhanced PCMs. Praveen Kumar et al. reported a temperature reduction of 16.5% and an increase in output power of 12.18% compared to an uncooled PV panel [13]. Similarly, Tuncer et al. utilized paraffin wax encapsulated in aluminum containers, resulting in an increase in electrical efficiency from 10.69% to 12.60%, with an average improvement of 9.84% [14]. Other studies have explored different PCM configurations and materials. Nada et al. examined three PV-PCM cooling scenarios and observed a temperature reduction of up to 10.6 °C when using a PCM enhanced with Al_2O_3 nanoparticles [15]. Baygi and Sadrameli employed polyethylene glycol (PEG 1000) as a PCM and reported a temperature decrease of approximately 15 °C, accompanied by an 8% increase in power output, with performance influenced by panel inclination angles [16].

More advanced system designs have also been investigated under controlled indoor conditions. Al-Aasam et al. conducted experiments using a solar simulator to evaluate a PVT-PCM system incorporating a twisted absorber tube and nanoparticle-enhanced PCM. The system achieved peak electrical and thermal efficiencies of 9.57% and 84.74%, respectively. The high thermal efficiency was attributed to additional heat gain from the exposed absorber surface [17]. In a related study, Bassam et al. examined a similar PVT-PCM configuration with nanoparticle enhancement and internally grooved cooling tubes.

Their system achieved maximum electrical and thermal efficiencies of 9.21% and 77.57%, respectively, with a peak power output of 15.25 W [18].

Horng et al. [19] tested a PV panel cooled with a PCM having a phase transition temperature of 36 °C in an indoor experiment under solar irradiance levels of up to 800 W/m^2. The results showed that the electrical efficiency increased by a maximum of 6.83% at an irradiance of 500 W/m^2 compared to a conventional PV panel. Xiang et al. [20] used longitudinal metal fins attached to the back of the PV panel and embedded within the PCM domain to enhance heat transfer in the PV-PCM system. Their results showed that the PV panel temperature decreased by 11.65 °C. Furthermore, coupling the PV-PCM setup with a forced cooling system led to an even greater reduction in panel temperature. The experiments were conducted under outdoor conditions with a maximum solar irradiance of 900 W/m^2 using a PCM with a phase transition temperature of 37 °C. The statistical review by Juwana et al. [21] demonstrated that the inclusion of the fin-PCM configuration achieved a maximum module temperature reduction of 15 °C, and that the simplified fin design was more practical.

Mehdi et al. [22] reported that the wind speed significantly reduced the PV module temperature by 12 °C, which led to an increase in the power and electrical efficiency of 7.2% and 6.5%, respectively, in an outdoor experimental investigation. Similarly, Ataman and Arslanoglu [23] found that low wind speeds below 0.5 m/s resulted in a temperature reduction of only 2–3 °C, whereas the temperature drop increased to as much as 7 °C when the wind speed approached 1 m/s. Hudisteanu et al. [24] numerically demonstrated the influence of wind speed on PV panels employing different passive fin-based cooling techniques, reporting power output improvements ranging from 1.85% to 7.71%, depending on the wind speed and its direction.

While existing research frequently explores natural and forced convection currents or passive PCM integration as distinct cooling solutions [25,26], there remains a notable lack of indoor experimental investigations quantifying the synergetic interaction between variable wind speeds and PCM-cooled photovoltaic panels. Current literature predominantly relies on numerical simulations or outdoor field tests, which often struggle to isolate the convective heat transfer coefficient due to uncontrolled ambient fluctuations [27,28].

In this study, indoor experiments were conducted to evaluate the thermal and electrical performance of PV panels integrated with PCM under varying irradiance levels and air movement conditions. Two PV-PCM configurations were investigated: a conventional flat rear PCM container (PV-2) and a modified extended-surface rear PCM container (PV-3). A reference PV panel without any cooling modification (PV-1) was also tested under the same operating conditions for comparison. The temperature variation and electrical performance of all three configurations were monitored across eighteen experimental runs. The study aimed to assess the effectiveness of using a PCM with a relatively high melting temperature in improving the thermal regulation and electrical output of PV panels under high irradiance conditions. By manipulating between natural and forced convection on the PV-PCM module in a controlled setting, researchers can isolate the influence of forced convection on the thermal latency provided by the phase change layer. This can significantly contribute to the understanding of air-side heat dissipation from the back of PV-PCM arrangements, as will be discussed for PV-2 and PV-3.

2. Materials and Methods

An indoor experimental setup, including the components illustrated in Figure 1, was developed to investigate the electrical and thermal performance of PV panels using solar simulator lamps. Three PV panels were tested. PV-1 served as the reference panel without any modifications, while PV-2 and PV-3 were equipped with PCM containers attached to

their backside to function as passive cooling systems. Prior to any modifications, all three panels were evaluated under identical conditions to verify manufacturer tolerances. The deviation in electrical efficiency was found to be less than 0.05%.

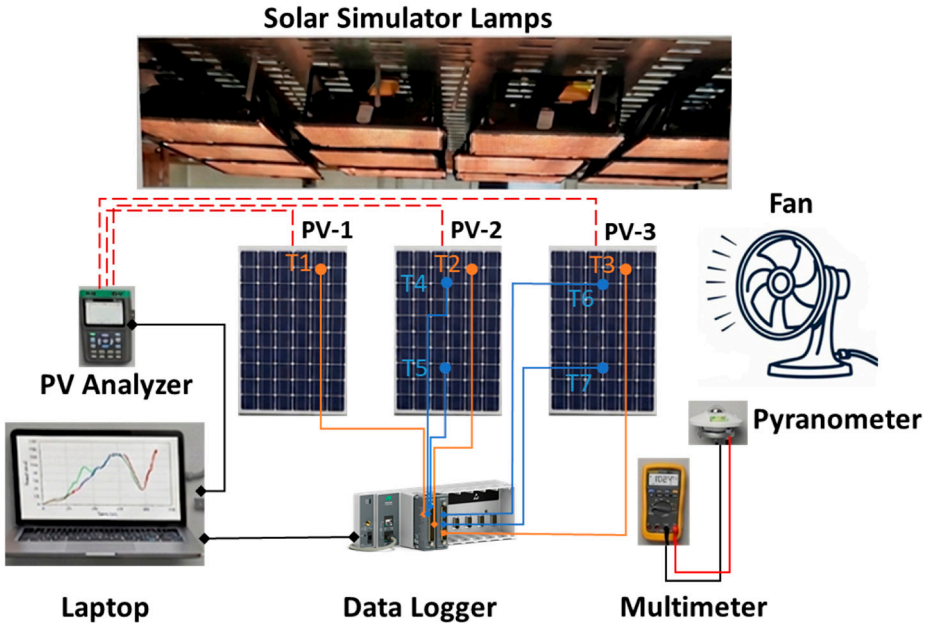


Figure 1. The main components of the indoor experimental setup.

All three PV panels were tested at three irradiance levels, 600, 800, and 1000 W/m^2, under two conditions: with and without a fan to simulate the cases of natural and forced convection currents. This resulted in six tests per panel and a total of eighteen tests, each lasting one to five hours until the panels reached steady-state or near-steady-state conditions.

2.1. Experimental Setup

Figure 2 illustrates the indoor experimental setup, highlighting the main devices and sensors used in this study. The solar panels (model CE-STG200W-01, CENSEE Ltd., Zhongshan, China) have a rated power of 20 W, and their full specifications are provided in Table 1. A solar simulator consisting of twelve 500 W halogen lamps was used to provide uniform and controlled irradiance. The lamps were regulated using three variable autotransformers to adjust the irradiance level incident on the panel surface. Solar irradiance was measured at nine fixed locations on each panel before start each experiment, and the three variable autotransformers (Figure 2) were adjusted accordingly to maintain irradiance deviations within 5% or less among the measurement points.

Table 1. The PV panel specifications under standard test conditions.

Parameter	Information
Model	CE-STG200W-01
Dimension (L × W × H)	390 × 300 × 17 mm
Maximum power (P_{max})	20 W
Voltage at P_{max}	5.7 V
Current at P_{max}	3.51 A
Open-circuit voltage	6.66 V
Short-circuit current	3.74 A
Working temperature	40~85 °C

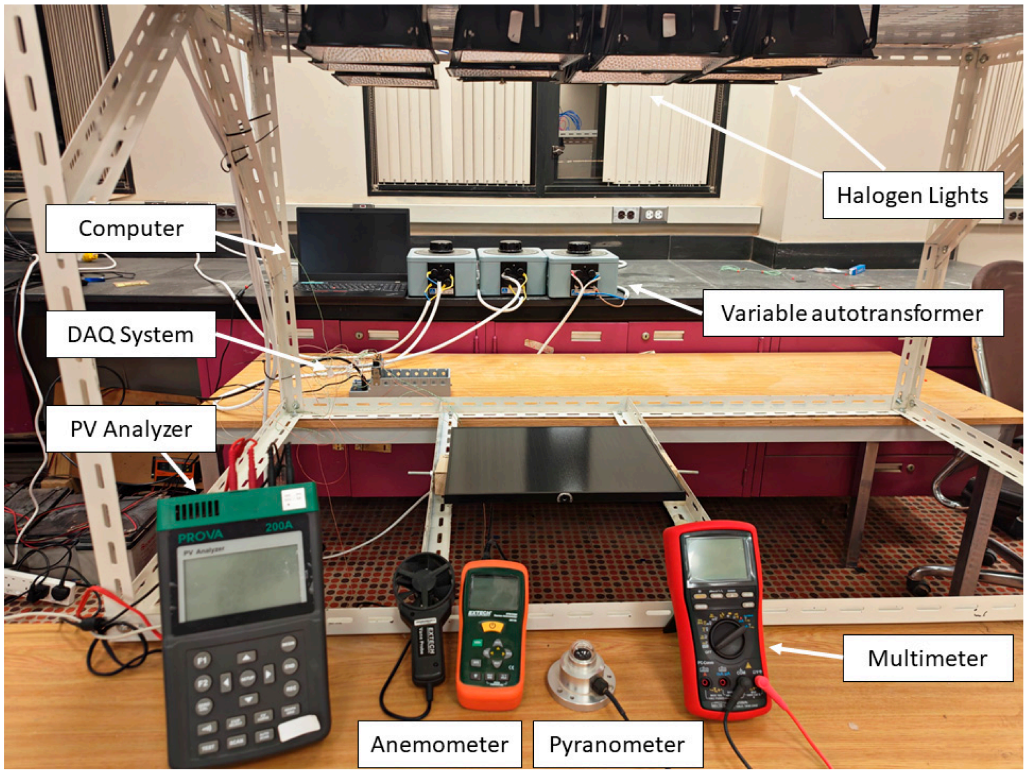


Figure 2. An experimental setup overview showing the indoor solar simulator system and the associated devices.

A Hukseflux LP02 pyranometer (Hukseflux Thermal Sensors, Delft, The Netherlands) [29], positioned at the same level as the PV panels, was used to measure the irradiance flux, with readings recorded via a multimeter. The PV panels were connected to a PROVA 200A PV analyzer (PROVA Instruments Inc., New Taipei City, Taiwan) [30], which recorded the maximum electrical power, along with the corresponding current and voltage values, at 5 min intervals for the first 30 min and at 10 min intervals thereafter.

Eight thermocouples (Omega SA3-K-120, Omega Engineering, Norwalk, CT, USA, and Labfacility Z2-K-1M, Labfacility Ltd., Sheffield, UK) were installed to measure the ambient temperature (T_{amb}) and panel temperatures (T1–T7) at various locations. Temperature data were continuously recorded using a National Instruments (NI, Austin, TX, USA) data acquisition system, consisting of a Compact DAQ chassis (NI cDAQ-9188) and a thermocouple input module (NI-9213). In addition, the average air velocity over the upper and lower surfaces of the PV panels was measured using an Extech AN100 thermo-anemometer (Extech Instruments, Nashua, NH, USA).

2.2. PV-PCM System Configurations

Figure 3 illustrates the three PV panels investigated in this study, shown during and after the addition of PCM and the installation of thermocouple locations. Three PV configurations were tested: a reference panel without PCM (PV-1), a rear flat container filled with PCM (PV-2), and a rear extended-surface container filled with PCM (PV-3). Thermocouples T1, T2, and T3 were attached to the back surface of PV-1, PV-2, and PV-3, respectively, at the top left area of each panel, as shown in Figure 3C. T4 and T5 were attached to the back surface of the PCM container of PV-2, with their average denoted as T2a. The same arrangement was applied to PV-3, where T6 and T7 were attached at similar positions, with their average denoted as T3a.



Figure 3. Preparing the PV-PCM modules and installing the thermocouples.

Figure 3A shows the PCM contained within two identical enclosures (26 × 26 cm^2 base area and 2 cm depth), fabricated from 2 mm thick 1050 aluminum sheets and attached to PV-2 and PV-3. The PCM containers were attached to the back of the PVs using thermal grease (with thermal conductivity of 1.93 W/m·K) to eliminate air gaps. Approximately 1.19 kg of Rubitherm RT-47 PCM (Rubitherm Technologies, Berlin, Germany), with a phase transition temperature range of 41–48 °C [31], was used. The detailed properties of the PCM are provided in Table 2.

The latent heat storage of Rubitherm RT-47 is concentrated around 47 °C, a temperature that generally exceeds the ambient conditions in hush conditions in cities such as Riyadh during most of the summer season. Selecting a PCM with a relatively high melting temperature helps keep the PV panel temperature near its phase change point for an

extended period, thereby enhancing thermal regulation. In addition, a high latent heat capacity is desirable to maximize energy absorption during the phase transition.

Table 2. Thermophysical properties of Rubitherm RT-47 phase change material [31].

Property	Value
Melting range (°C)	41–48
Congealing range (°C)	48–41
Main melting peak (°C)	47
Main congealing peak (°C)	46
Heat storage capacity (kJ/kg)	160 ± 7.5%
Specific heat capacity (kJ/kg·K)	2
Thermal conductivity—both phases (W/m·K)	0.2
Density—solid at 15 °C (kg/L)	0.88
Density—liquid at 80 °C (kg/L)	0.77
Volume expansion (%)	12
Flash point (°C)	>180

PV-2 was simply covered with a 2 mm thick flat aluminum sheet, as shown in Figure 3B. However, as reported in the literature, a PCM-filled back container may, under certain conditions, restrict heat dissipation from the rear surface of the PV panel [9,32].

To overcome this limitation, the PV-3 cover was further modified by incorporating extended aluminum surfaces filled with PCM, as illustrated in Figure 3A,B. This design consists of 20 rectangular prism compartments (2 cm wide × 4 cm long × 4 cm high each), allowing for the addition of an extra 0.53 kg of PCM and increasing the rear surface area exposed to the surroundings by approximately 240%. The modified PV-3 cover was filled with PCM prior to sealing as shown in Figure 3A. Aluminum supports were used to compress the PCM containers to the back of the PVs, as shown in Figure 3C.

2.3. Performance Indicators

The PV analyzer determines the maximum power output and generates the current–voltage (I–V) curve under the given conditions by applying artificial loads to the panel. The maximum power (P), along with the corresponding short-circuit current and open-circuit voltage, is recorded. The electrical efficiency (η) of the panel is then calculated as follows:

$$\eta = \frac{P}{G\,A} \tag{1}$$

where the G is the measured solar irradiance and A is the panel area. To calculate the average electrical efficiency, the weighted average of the electrical power is used as follows:

$$\eta_{ave} = \frac{\sum_0^t P\Delta t}{G\,A} \tag{2}$$

The PV analyzer and the pyranometer each have an accuracy of 1%, resulting in an overall uncertainty of 1.41% in the calculated electrical efficiency after applying the following uncertainty rule [33]:

$$\varepsilon_\eta = \left[\left(\frac{\partial \eta}{\partial P_{elec}} \times \varepsilon(P_{elec}) \right)^2 + \left(\frac{\partial \eta}{\partial G} \times \varepsilon(G) \right)^2 \right]^{\frac{1}{2}} \tag{3}$$

3. Results and Discussion

3.1. Thermal Performance of PCM-Cooled PV Panels

The temperatures measured at thermocouple measurement points T1, T2, and T3 for PV-1, PV-2, and PV-3, respectively, are presented in Figure 4 for all experimental cases, together with the corresponding ambient temperatures. It should be noted that T1–T3 were selected primarily as comparative indicators among the three panels, as T2–T3 were positioned near to the PCM container. T2a represents the average of temperature measurements T4 and T5 measured at the back surface of the PCM container of PV-2. Similarly, T3a represents the average of T6 and T7 measured at the same locations for PV-3. These average temperatures provide a more representative indication of the phase change process at the rear surface of the PCM container, as will be discussed later in Figure 5.

Figure 4a–f show that the thermal performance of the panels was significantly influenced by air movement. Therefore, the results are presented in pairs, comparing natural convection and forced convection conditions side by side. The forced convection was achieved using a fan, producing airflow velocities of approximately 1.5 m/s above the panels and 0.9 m/s below them. These conditions represent a moderate forced convection regime that may simulate practical outdoor wind effects.

At a low irradiance level of 600 W/m^2, no significant improvement in panel temperature reduction was observed for PV-2 and PV-3 compared with the reference panel PV-1 under natural convection conditions, as shown in Figure 4a. However, T3 exhibited a noticeable lower temperature over extended operation periods, reaching up to 4.3 °C lower than T2 after 280 min. This lower T3 value can be attributed to the increased heat dissipation surface area incorporated in the PV-3 configuration, which enhanced and sustained the natural convection heat transfer mechanism.

Under forced convection at the same irradiance level of 600 W/m^2, the panels' surface temperatures decreased by approximately 11 °C compared to the natural convection tests, as shown in Figure 4b. It was noticed that T3 was slightly higher than T1 and T2 for most of the operating period. This is likely due to the higher ambient temperature recorded during the PV-3 test, which directly contributed to its elevated temperature response.

As illustrated in Figure 4b, under forced convection conditions, the average ambient temperature during the first 80 min of the PV-3 experiment was approximately 1.9 °C higher than that of the PV-2 experiment. Although a similar difference in ambient temperature was observed under natural convection conditions (Figure 4a), its impact was more pronounced in the forced convection case. As a result, the elevated ambient temperature contributed more significantly to the increase in PV-3 temperature (T3) under forced convection.

At a higher irradiance level of 800 W/m^2 combined with limited air movement, the beneficial effect of incorporating PCM into PV-2 and PV-3 became more evident. Considerable reductions in T2 and T3 compared to T1 were observed, particularly during the first hour of operation, as illustrated in Figure 4c. During this period, T2 and T3 were noticeably lower than T1. The reference panel PV-1 reached a maximum temperature of 69.84 °C, whereas PV-2 and PV-3 reached lower maximum temperatures of 63.8 °C and 65.53 °C, respectively. In contrast, under forced convection conditions, the cooling effect was less pronounced, as shown in Figure 4d, with a maximum temperature difference of only 2.74 °C between the panels.

At the highest irradiance level of 1000 W/m^2 under natural convection, T1 recorded the highest value of 76.8 °C after the first 40 min of operation, compared with corresponding temperatures of 65.5 °C and 68.4 °C for T2 and T3, respectively. This confirms that the PCM in PV-2 and the extended-surface PCM in PV-3 were effective in maintaining a lower surface temperature than PV-1, particularly during this period. The flat PCM container of PV-2 gradually lost its cooling effectiveness over time, while the extended-surface configuration

of PV-3 consistently maintained lower panel temperatures throughout the test. This clearly demonstrates that the PV-3 configuration provided a more durable and effective thermal management solution, as shown in Figure 4c,e. Under forced convection, however, at the same irradiance level, the panel temperatures were approximately 20 °C lower compared to natural convection conditions. The effect of forced convection was more pronounced at higher irradiance levels. It is worth noting that the ambient temperature was maintained at approximately 25 °C during the indoor tests, which enhanced the effectiveness of forced convection by increasing the temperature difference between the panel surface and the surrounding air.

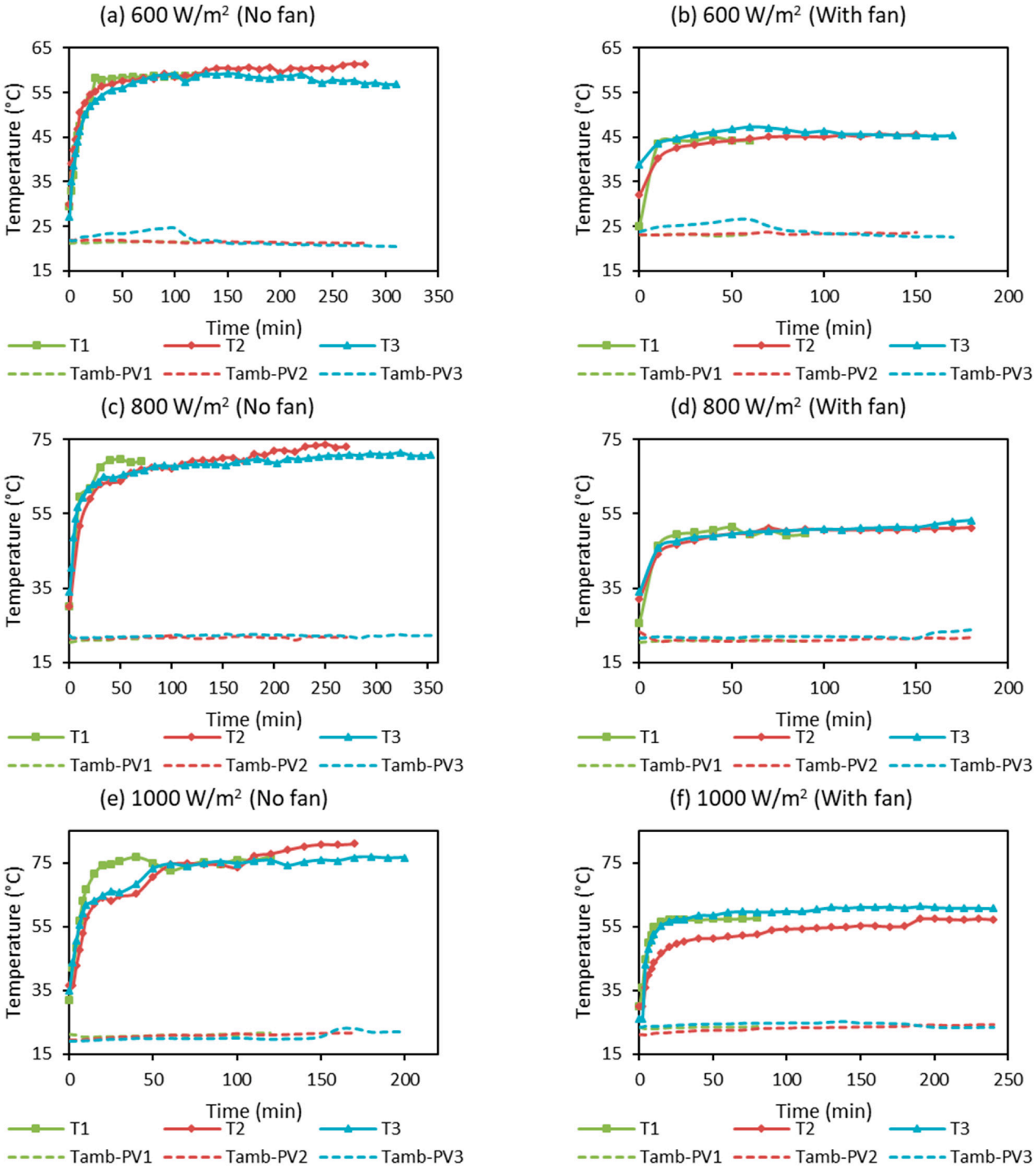


Figure 4. The time variations in the temperature of the PV-1, PV-2, and PV-3 panels under different test conditions.

Figure 5 illustrates the temporal variation in the average PCM container rear surface temperatures T2a and T3a for PV-2 and PV-3 under all investigated operating conditions. The results clearly demonstrate that the modified PCM container design of PV-3 substantially reduced the temperature at the back surface of the PCM container compared to the flat surface of PV-2, indicating more effective heat dissipation to the surrounding environment, which acts as the heat sink in the cooling process. This improvement was particularly evident in natural convection experiments, as shown in Figure 5a,c,e.

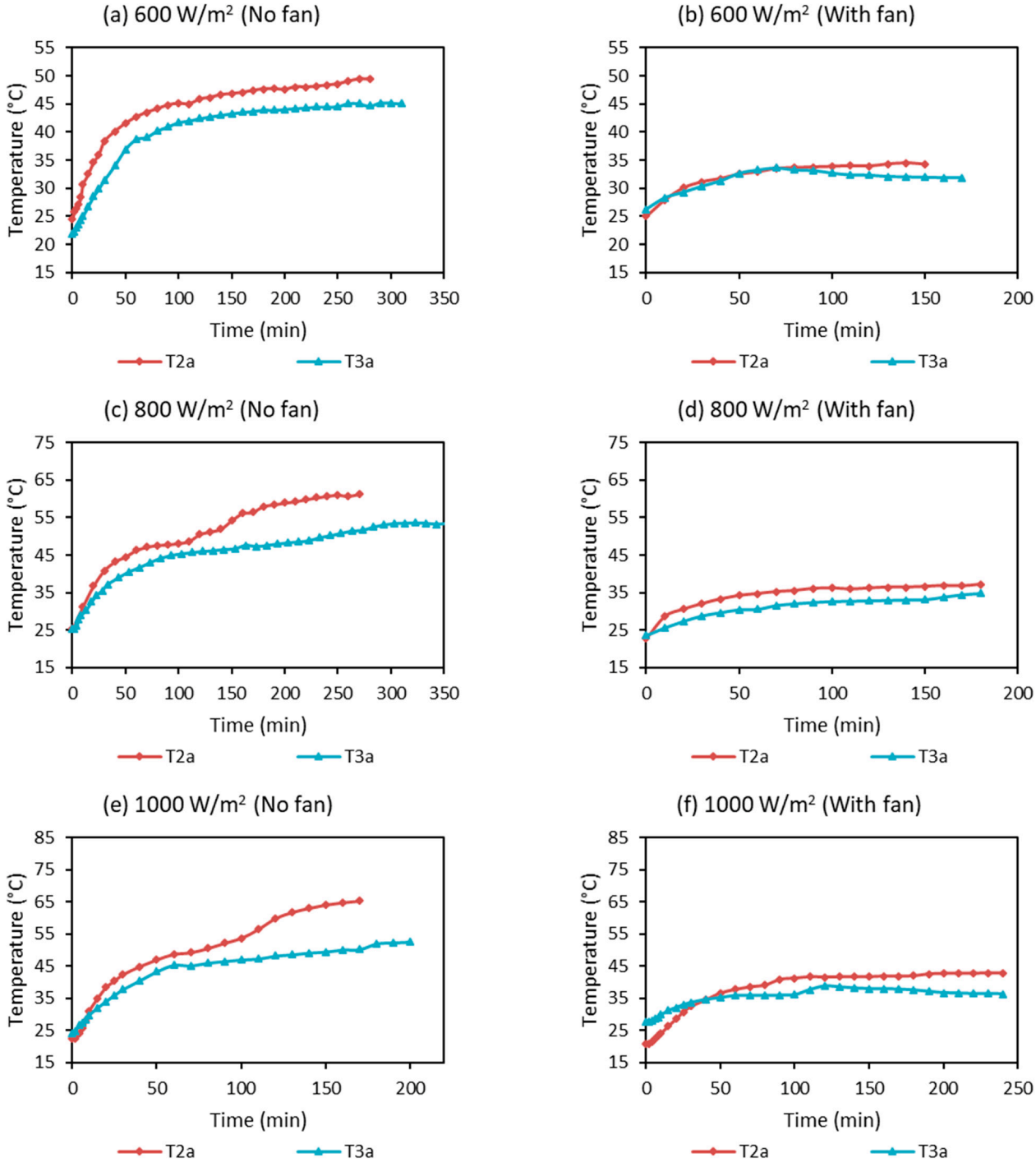


Figure 5. The average rear surface temperatures of the PCM for PV-2 and PV-3 under different test conditions.

In the PV-3 configuration, the 240% increase in extended surface area and the 44% increase in PCM mass relative to PV-2 contributed to a considerable reduction in the back-surface temperature of the PV-3 container. However, simply increasing the amount of PCM in a conventional container, as in PV-2, results in a thicker PCM layer, which does not necessarily enhance PV electrical performance. This effect is particularly evident under natural convection conditions and has been reported in several previous studies [34,35]. Increasing PCM thickness does not lead to continuous performance improvement. Beyond a certain thickness, the PCM layer begins to act as a thermal insulator rather than an effective heat sink. As a result, the PCM located farther from the PV module may not fully melt, limiting heat transfer and reducing the overall thermal regulation capability of the system.

In the present study, as the irradiance level increases, the difference in back surface temperature between T2a and T3a becomes more pronounced, reaching a maximum of 15 °C after 170 min of operation at an irradiance level of 1000 W/m^2, under natural convection as shown in Figure 5e. It is worth noting that the trend of T3a is different than T2a, which indicates that the temperature reduction is primarily due to the extended surface area associated with the PV-3 container.

Under forced convection at 600 W/m^2, no clear advantage of PV-3 over PV-2 was observed. At this low irradiance level, the panel surface temperature remains below the PCM main melting point of 47 °C, as shown in Figure 4b, and therefore, the phase change mechanism was not effectively activated. At irradiance levels 800 and 1000 W/m^2 under forced convection, T3a remained generally lower than T2a throughout most of the operating period. The low indoor ambient temperatures of 20–25 °C likely enhanced the cooling effect under forced convection and influenced the thermal behavior of the panels.

When the rear surface temperature of the PCM container falls within the melting range of 41–48 °C, the PCM absorbs incoming heat as latent heat, serving as the main cooling mechanism. It can also be noticed that T2a in the PV-2 configuration exceeded the nominal PCM melting temperature of 47 °C after approximately 80 min and 50 min, respectively, as shown in Figure 5c,e at 800 and 1000 W/m^2 under natural convection. This observation strongly suggests that the PCM within the containers had completely melted in both cases at the given times.

3.2. Electrical Performance of PCM-Cooled PV Panels

Figure 6 presents the temporal variations in the open-circuit voltage (Voc) and short-circuit current (Isc) for all panels under the different test conditions. As expected, the open-circuit voltage exhibited an inverse relationship with the panel surface temperature, consistent with the well-established temperature dependence of photovoltaic cells [36]. An increase in cell temperature adversely affected solar cell performance, primarily due to the exponential rise in the reverse saturation current density, which led to a significant reduction in the open-circuit voltage.

In contrast, the short-circuit current exhibited the expected increase with rising operating temperature [37]. Furthermore, the more uniform temperature distribution across the PV cells in PV-1 helped reduce short-circuit current losses associated with current mismatch. In series-connected photovoltaic cells, the overall string current is limited by the cell producing the lowest current [38]. Therefore, non-uniform temperature distributions or localized thermal gradients can lead to variations in the electrical characteristics of individual cells, resulting in current mismatch losses and a reduction in overall module performance [39].

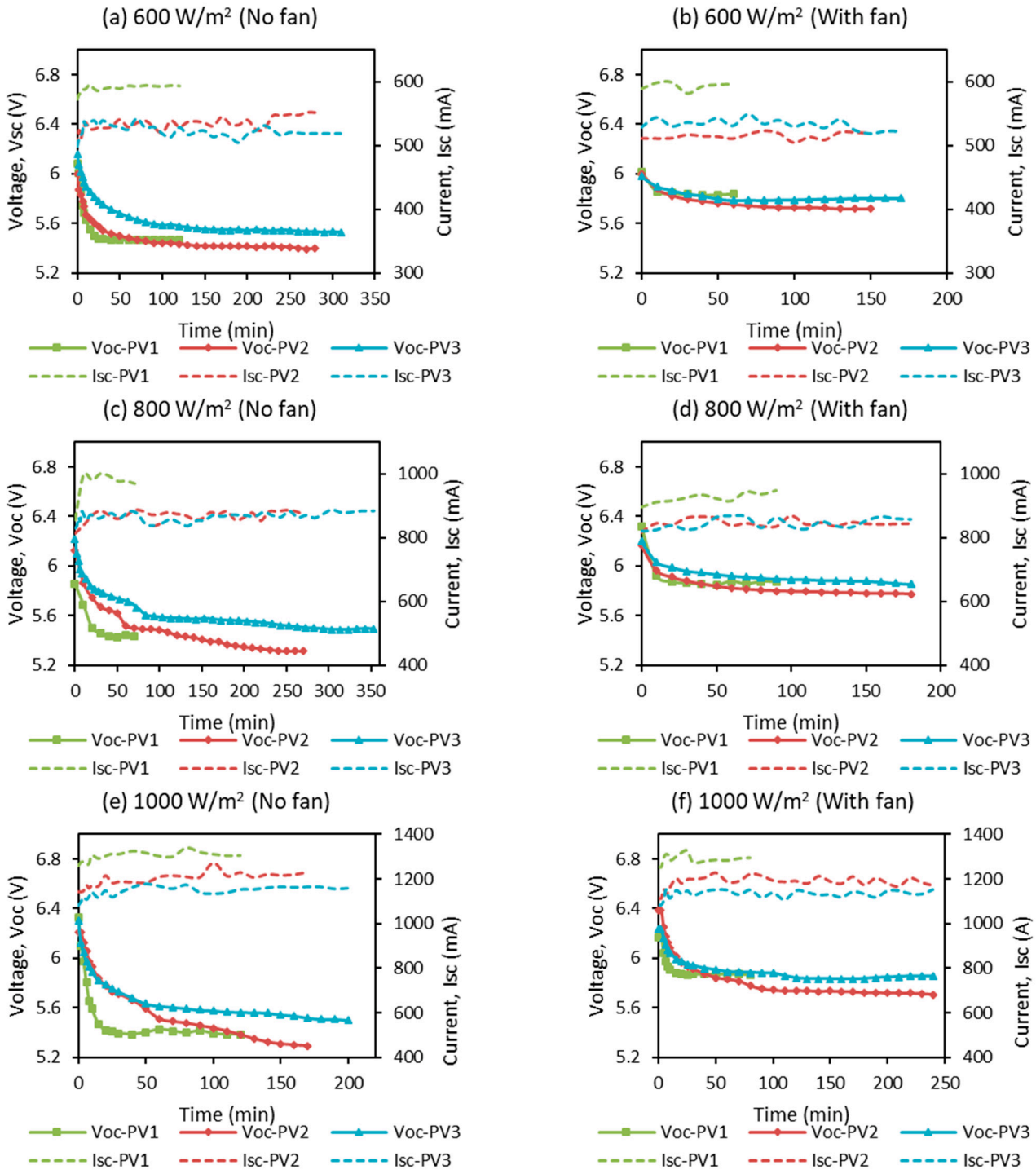


Figure 6. The time variations in the open-circuit voltage and short-circuit current under different test conditions.

For the reference panel (PV-1) under natural convection, the open-circuit voltage (Voc) decreased more rapidly during the initial stage of the test than that of PV-2 and PV-3. This behavior can be attributed to the absence of PCM cooling, which resulted in a faster increase in the panel surface temperature. In contrast, the short-circuit current (Isc) increased with the rise in temperature and benefited from the more uniform temperature distribution across the PV-1 cells. For example, at an irradiance of 1000 W/m^2 under natural convection, PV-1 recorded the highest Isc among all panels, reaching 1340 mA after 80 min of operation, compared with 1210 mA and 1174 mA for PV-2 and PV-3, respectively. However, at the

same operating time, PV-3 exhibited the highest Voc, reaching 5.59 V, whereas PV-1 and PV-2 recorded 5.39 V and 5.47 V, respectively.

A comparison of the open-circuit voltage under natural and forced convection conditions, as shown in Figure 6, reveals that Voc was consistently lower under natural convection. This finding indicates the strong dependence of Voc on panel surface temperature, with elevated temperatures leading to a reduction in voltage output. Among the tested configurations, PV-3 consistently exhibited the highest Voc under both natural and forced convection conditions across all irradiance levels.

The output power and electrical efficiency of PV-1, PV-2, and PV-3 are shown in Figure 7 under various irradiance levels and convection conditions. In general, the output power and efficiency of the PV panels increased with increasing irradiance level.

With no fan assistance (natural convection), increasing the irradiance from 600 to 800 W/m^2 improved the average electrical efficiency of PV-1 from 3.98% to 5.10% over the study period. However, a further increase in irradiance to 1000 W/m^2 resulted in only a marginal improvement, with the efficiency reaching 5.17%. A similar trend was observed under forced convection conditions when a fan was used. This behavior can be attributed to the elevated operating temperatures encountered at higher irradiance levels (approximately 75 °C), which adversely affect the electrical performance of the PV module and partially offset the beneficial effect of the increased solar irradiance.

Under natural convection conditions, as shown in Figure 7a,c,e, PV-3 consistently produced higher output power than both PV-1 and PV-2. This is consistent with the temperature results discussed in Section 3.1, where the extended-surface PCM container of PV-3 provided a more effective cooling performance compared to PV-2. As shown by Equation (1), variations in electrical efficiency were typically equivalent to variations in electrical power. Therefore, the improvement in electrical efficiency was more pronounced at an irradiance level of 1000 W/m^2, as the higher panel temperatures at this level allowed the PCM to contribute more effectively to cooling through latent heat absorption.

At an irradiance of 1000 W/m^2 under natural convection, as shown in Figure 7e, PV-3 achieved the highest enhancement in electrical power, with maximum increases of 12.05% and 7.38% compared to PV-1 and PV-2, respectively, after the first 40 min of operation. Throughout the entire study period, PV-3 consistently exhibited the best performance, providing average power enhancements of 7.06% and 5.35% relative to PV-1 and PV-2, respectively.

In contrast, PV-2 initially outperformed PV-1 under natural convection at all irradiance levels. However, after approximately 50–80 min of operation, PV-2 gradually lost this advantage and eventually exhibited the lowest electrical power output and efficiency among the three panels. For instance, at an irradiance of 800 W/m^2 under natural convection, the average electrical power generated by PV-2 was 5.45% lower than that of PV-1 over the study period. This decline can be attributed to the reduced effectiveness of the PCM in the plain container over time, resulting from restricted heat dissipation from the rear side of the panel, as illustrated by the discussion in Figure 5.

On the other hand, under forced convection conditions, the output power and electrical efficiency of all three panels increased compared to their natural convection counterparts at the same irradiance level, as shown in Figure 7, which is directly attributed to the reduction in panel surface temperature. However, the difference in performance among PV-1, PV-2, and PV-3 was minimal compared to natural convection cases, as forced convection was the dominant cooling mechanism, reducing the role of the PCM in the overall cooling process.

Under forced convection conditions, PV-1 exhibited the highest overall performance in terms of both output power and electrical efficiency at the lowest irradiance level of 600 W/m^2, achieving average improvements of 3.54% and 2.29% compared to PV-2 and

PV-3, respectively. At an irradiance of 800 W/m^2, PV-1 and PV-3 demonstrated comparable performance, with PV-3 achieving only a marginally higher average efficiency by 0.62% relative to PV-1. At 1000 W/m^2, PV-2 initially exhibited the best performance during the first 50 min of operation. However, as the operating time increased, PV-1 outperformed both PV-2 and PV-3, recording average improvements of 2.93% and 2.53%, respectively, over the study period.

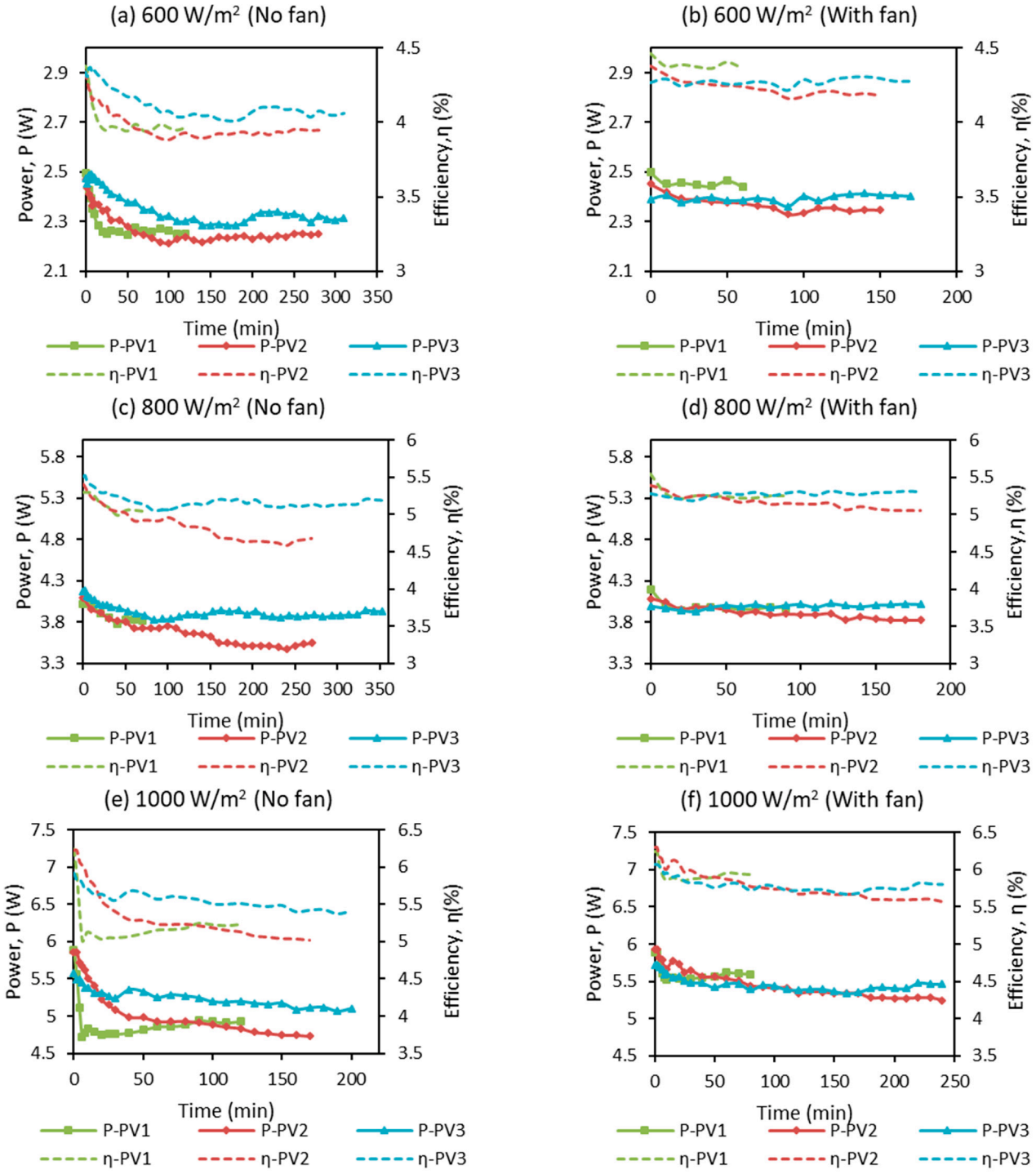


Figure 7. The time variations in the output power and electrical efficiency under different test conditions.

Several factors contributed to the lower measured efficiencies. First, the spectral distribution and illumination characteristics of the solar simulator may differ from the AM1.5 solar spectrum used for standard PV efficiency ratings. Second, the PV panels

operated at temperatures significantly higher than the STC reference temperature of 25 °C, which adversely affected their electrical performance. It should also be noted that the objective of the present study was to compare the relative performance of the reference panel and the PCM-cooled configurations under identical operating conditions. Therefore, the key findings are based on the comparative improvements in electrical performance among the tested configurations rather than on the absolute efficiency values themselves.

4. Conclusions

This study experimentally investigated the thermal and electrical performance of three PV panel configurations—a reference panel without PCM (PV-1), a flat back-container PCM panel (PV-2), and a rear extended-surface container filled with PCM (PV-3)—under indoor solar simulation at irradiance levels of 600, 800, and 1000 W/m^2, under both natural and forced convection conditions. The selected PCM was Rubitherm RT-47, with a melting temperature range of 41–48 °C. The main conclusions drawn from this study are as follows:

- The modified PCM container in PV-3 enhanced heat dissipation to the surrounding environment, resulting in significantly lower back-surface temperatures compared to PV-2. This improvement was most pronounced under natural convection and became more evident at higher irradiance levels, with the temperature difference between T2a and T3a reaching up to 15 °C after 170 min of operation at 1000 W/m^2.
- Under natural convection at an irradiance of 1000 W/m^2, PV-3 demonstrated the best electrical performance, achieving maximum power enhancements of 12.05% and 7.38% compared with PV-1 and PV-2, respectively, during the first 40 min of operation.
- Over the entire study period, PV-3 maintained its performance advantage, delivering average power increases of 7.06% and 5.35% relative to PV-1 and PV-2, respectively, highlighting its superior thermal management capability and effectiveness under high-irradiance conditions.
- Under forced convection, the performance differences among the three configurations were relatively small because forced convection dominated the cooling process, reducing the contribution of the PCM.

The passive extended-surface PV cooling system filled with PCM shows strong potential. In this study, it was evaluated under controlled indoor conditions. It is recommended that future work extend this concept to large-scale outdoor PV systems to assess its real-world performance. Such investigations should consider practical environmental challenges, including dust accumulation on the extended surfaces, humidity and corrosion effects, wind variability, and long-term thermal cycling impacts, which may influence both cooling effectiveness and system durability.

Author Contributions: T.A.: Conceptualization, Methodology, Software, Formal analysis, Investigation, Data curation, Writing—original draft, Funding acquisition. Project administration. M.B.E.: Conceptualization, Methodology, Software, Formal analysis, Investigation, Data curation, Writing—original draft, Writing—review & editing, Visualization, Supervision. All authors have read and agreed to the published version of the manuscript.

Funding: This research was funded by Waed Program (W25-49), King Saud University, Riyadh, Saudi Arabia.

Institutional Review Board Statement: Not applicable.

Informed Consent Statement: Not applicable.

Data Availability Statement: The original contributions presented in this study are included in the article. Further inquiries can be directed to the corresponding author.

Acknowledgments: The authors would like to extend their appreciation to the Deanship of Scientific Research at King Saud University for funding this work through Waed Program (W25-49).

Conflicts of Interest: The authors declare no conflicts of interest.

Nomenclature

A	Area (m^2)
C	Specific heat (J/kg K)
G	Solar irradiance (W/m^2)
I	Current (A)
I_{max}	Current at maximum power
P	Electrical power (W)
PVT	Photovoltaic thermal
T	Temperature (°C)
t	Time (s)
V	Voltage (V)
V_{max}	Voltage at maximum power
Greek Letters	
η	Efficiency (%)

Abbreviations

PCM	Phase change material
PV	Photovoltaic
PV-1	Reference PV panel without PCM
PV-2	PV panel with PCM
PV-3	PV panel with PCM and fins
Subscript	
amb	Ambient
max	Maximum
oc	Open circuit
sc	Short circuit
th	Thermal

References

1. Kassar, R.E.; Takash, A.A.; Faraj, J.; Khaled, M.; Ramadan, H.S. Phase change materials for enhanced photovoltaic panels performance: A comprehensive review and critical analysis. *Energy Built Environ.* **2025**, *6*, 655–675. [CrossRef]
2. Singh, R.; Sharma, M.; Yadav, K. Degradation and reliability analysis of photovoltaic modules after operating for 12 years: A case study with comparisons. *Renew. Energy* **2022**, *196*, 1170–1186. [CrossRef]
3. Castro, R.; Teixeira, I. Heat Waves and Photovoltaic Performance: Modelling, Sensitivity, and Economic Impacts in Portugal. *Sustainability* **2025**, *18*, 289. [CrossRef]
4. Elsheniti, M.B.; Zaheer, S.; Zeitoun, O.; Fouly, A.; Abdo, H.S.; Almutairi, Z. An experimental assessment of a solar PVT-PCM thermal management system in severe climatic conditions. *J. Build. Eng.* **2024**, *97*, 110691. [CrossRef]
5. Harmailil, I.O.; Sultan, S.M.; Fudholi, A.; Mohammad, M.; Tso, C.P. Enhancing PV Module Efficiency Through Fins-and-Tubes Cooling: An Outdoor Malaysian Case Study. *Processes* **2025**, *13*, 2812. [CrossRef]
6. Harmailil, I.O.; Sultan, S.M.; Tso, C.P.; Fudholi, A.; Mohammad, M.; Ibrahim, A. The State of the Art of Photovoltaic Module Cooling Techniques and Performance Assessment Methods. *Symmetry* **2024**, *16*, 412. [CrossRef]
7. Alikhan, A.H.; Kazemi, M.; Soroush, H. Enhanced performance of photovoltaic thermal module and solar thermal flat plate collector connected in series through integration with phase change materials: A comparative study. *Therm. Sci. Eng. Prog.* **2024**, *47*, 102305. [CrossRef]
8. Elsheniti, M.B.; Hemedah, M.A.; Sorour, M.M.; El-Maghlany, W.M. Novel enhanced conduction model for predicting performance of a PV panel cooled by PCM. *Energy Convers. Manag.* **2020**, *205*, 112456. [CrossRef]

9. Colarossi, D.; Principi, P. Indoor and Outdoor Performance of an Enhanced Photovoltaic Panel through Graphene/Fins/Phase Change Materials. *Appl. Sci.* **2021**, *11*, 8807. [CrossRef]
10. Liu, J.; Zhong, W.; Lv, Z.; Li, C.; Liu, Y. Thermal management in EV wireless charging: Breakthroughs, challenges, and next-generation cooling strategies. *DeCarbon* **2025**, *10*, 100133. [CrossRef]
11. Elsheniti, M.B.; Zaheer, S.; Zeitoun, O.; Alshehri, H.; AlRabiah, A.; Almutairi, Z. Experimental Evaluation of a Solar Low-Concentration Photovoltaic/Thermal System Combined with a Phase-Change Material Cooling Technique. *Appl. Sci.* **2022**, *13*, 25. [CrossRef]
12. Liu, L.; Niu, J.; Wu, J.-Y. Improving energy efficiency of photovoltaic/thermal systems by cooling with PCM nano-emulsions: An indoor experimental study. *Renew. Energy* **2023**, *203*, 568–582. [CrossRef]
13. PraveenKumar, S.; Agyekum, E.B.; Kumar, A.; Velkin, V.I. Performance evaluation with low-cost aluminum reflectors and phase change material integrated to solar PV modules using natural air convection: An experimental investigation. *Energy* **2023**, *266*, 126415. [CrossRef]
14. Tuncer, A.D.; Khanlari, A.; Aytaç, İ.; Çiftçi, E.; Sözen, A.; Variyenli, H.İ. Passive Thermal Management of Photovoltaic Panel by Using Phase Change Material-Filled Aluminum Cans: An Experimental Study. *Heat Transf. Res.* **2022**, *53*, 73–86. [CrossRef]
15. Nada, S.A.; El-Nagar, D.H.; Hussein, H.M.S. Improving the thermal regulation and efficiency enhancement of PCM-Integrated PV modules using nano particles. *Energy Convers. Manag.* **2018**, *166*, 735–743. [CrossRef]
16. Mousavi Baygi, S.R.; Sadrameli, S.M. Thermal management of photovoltaic solar cells using polyethylene glycol 1000 (PEG1000) as a phase change material. *Therm. Sci. Eng. Prog.* **2018**, *5*, 405–411. [CrossRef]
17. Al-Aasam, A.B.; Ibrahim, A.; Sopian, K.; Abdulsahib, M.B.; Dayer, M. Nanofluid-based photovoltaic thermal solar collector with nanoparticle-enhanced phase change material (Nano-PCM) and twisted absorber tubes. *Case Stud. Therm. Eng.* **2023**, *49*, 103299. [CrossRef]
18. Bassam, A.M.; Sopian, K.; Ibrahim, A.; Fauzan, M.F.; Al-Aasam, A.B.; Abusaibaa, G.Y. Experimental analysis for the photovoltaic thermal collector (PVT) with nano PCM and micro-fins tube nanofluid. *Case Stud. Therm. Eng.* **2023**, *41*, 102579. [CrossRef]
19. Chia Zhi, H.; Mohd Afzanizam Mohd, R.; Jayaprakash, P.; Nurfarhana, S.; Safarudin Ghazali, H.; Faridah, H. The Performance Evaluation of Photovoltaic Integrated Organic Phase Change Material in a Single Container using Indoor Solar Simulator. *J. Adv. Res. Fluid Mech. Therm. Sci.* **2023**, *109*, 168–183. [CrossRef]
20. Xiang, S.; Li, D.; Sun, X. Improved efficiency of photovoltaic/thermal system with phase change materials: Experimental study. *Appl. Therm. Eng.* **2026**, *285*, 129273. [CrossRef]
21. Juwana, W.E.; Racmanto, R.A.; Ubaidillah; Trisnoaji, Y.; Prasetyo, S.D.; Arifin, Z. The role of fin–PCM integration in enhancing photovoltaic performance. *Green Technol. Sustain.* **2026**, *4*, 100306. [CrossRef]
22. Mehdi, M.; Ammari, N.; Alami Merrouni, A.; Benazzouz, A.; Dahmani, M. Experimental investigation on the effect of wind as a natural cooling agent for photovoltaic power plants in desert locations. *Case Stud. Therm. Eng.* **2023**, *47*, 103038. [CrossRef]
23. Ataman, A.; Arslanoğlu, N. Investigation of the cooling effect of wind on rooftop PV power plants. *Case Stud. Therm. Eng.* **2024**, *63*, 105295. [CrossRef]
24. Hudișteanu, S.V.; Țurcanu, F.E.; Cherecheș, N.-C.; Popovici, C.-G.; Verdeș, M.; Ancaș, D.-A.; Hudișteanu, I. Effect of Wind Direction and Velocity on PV Panels Cooling with Perforated Heat Sinks. *Appl. Sci.* **2022**, *12*, 9665. [CrossRef]
25. Hossam, N.; Abd El-Hamid, M.; Gamal, M.; Fatouh, M. Thermal management of photovoltaic modules using phase change materials: Experimental and numerical investigations. *Appl. Therm. Eng.* **2025**, *279*, 127645. [CrossRef]
26. Madurai Elavarasan, R.; Pugazhendhi, R.; Shafiq, S.; Gangatharan, S.; Nadarajah, M.; Shafiullah, G.M. Efficiency enhancement of PV panels with passive thermal management using PCM: An exhaustive review on materials, designs and effective techniques. *Appl. Energy* **2025**, *382*, 125217. [CrossRef]
27. Raza, S.; Farooq, A.; Shehzad, M.S.; Hussain, W.; Abbas, Z.; Im, I.-T. A CFD analysis of photovoltaic panel cooling: A review. *Int. J. Air-Cond. Refrig.* **2026**, *34*, 2. [CrossRef]
28. Hassanian, R.; Yeganeh, N.; Riedel, M. Wind Velocity and Forced Heat Transfer Model for Photovoltaic Module. *Fluids* **2024**, *9*, 17. [CrossRef]
29. HKUC Sensor Technology. Hukseflux Pyranometer. Available online: https://www.hukseflux.com/uploads/inline/LP02_manual_v2008_DISCONTINUED.pdf (accessed on 15 March 2026).
30. PROVA 200A. PV Analyzer PROVA-200A Datasheet. Available online: https://www.prova.com.tw/img/download/200A-Data%20Sheet-2015.pdf (accessed on 15 March 2026).
31. Rubitherm. RUBITHERM® RT47 Datasheet. Available online: https://www.rubitherm.eu/media/products/datasheets/Techdata_-RT47_EN_09102020.PDF (accessed on 15 March 2026).
32. Zheng, C.-L.; Yuan, K.-H.; Chen, Y.-B. Enhanced photovoltaic performance via press-fitted phase change material tubes for passive thermal management. *Appl. Therm. Eng.* **2026**, *298*, 130938. [CrossRef]
33. Holman, J.P. *Experimental Methods for Engineers*, 8th ed.; McGraw-Hill: New York, NY, USA, 2011.

34. Mazzeo, D.; Ogliari, E.; Lucchini, A.; Dolara, A.; Carraretto, I.M.; Manzolini, G.; Colombo, L.P.M.; Leva, S. Integration of photovoltaic modules with phase change materials: Experimental testing, model validation and optimization. *Energy* **2025**, *319*, 134959. [CrossRef]
35. Mansir, I.B. The effect of PCM layer thickness and coolant mass flow rate on the efficiency of a double-channel photovoltaic/thermal-PCM system: Numerical and artificial neural network analysis. *Eng. Anal. Bound. Elem.* **2024**, *159*, 229–236. [CrossRef]
36. Singh, P.; Ravindra, N.M. Temperature dependence of solar cell performance—An analysis. *Sol. Energy Mater. Sol. Cells* **2012**, *101*, 36–45. [CrossRef]
37. Adeeb, J.; Farhan, A.; Al-Salaymeh, A. Temperature Effect on Performance of Different Solar Cell Technologies. *J. Ecol. Eng.* **2019**, *20*, 249–254. [CrossRef] [PubMed]
38. Shen, X.; Fan, H.; Wang, S.; Li, L.; Tang, C.; Zhang, L.; Li, H.; Qiao, Y.; Zhang, C.; Li, C.; et al. Mechanism analysis and quantitative evaluation of series mismatch losses in photovoltaic modules. *Energy Rep.* **2026**, *15*, 109078. [CrossRef]
39. Segbefia, O.K. Temperature profiles of field-aged photovoltaic modules affected by optical degradation. *Heliyon* **2023**, *9*, e19566. [CrossRef] [PubMed]

Disclaimer/Publisher's Note: The statements, opinions and data contained in all publications are solely those of the individual author(s) and contributor(s) and not of MDPI and/or the editor(s). MDPI and/or the editor(s) disclaim responsibility for any injury to people or property resulting from any ideas, methods, instructions or products referred to in the content.